Maximally localized Wannier functions in antiferromagnetic MnO within the FLAPW formalism

Michel Posternak* and Alfonso Baldereschi
Institute of Theoretical Physics, Swiss Federal Institute of Technology Lausanne, EPFL, PHB-Ecublens, CH-1015 Lausanne, Switzerland

Sandro Massidda
Istituto Nazionale di Fisica della Materia–Dipartimento di Fisica, Università di Cagliari, Cittadella Universitaria, I-09042 Monserrato (CA), Italy

Nicola Marzari
Department of Materials Science and Engineering, Massachusetts Institute of Technology, Cambridge, Massachusetts 02139-4307
(Received 3 October 2001; published 30 April 2002)

We have calculated the maximally localized Wannier functions of MnO in its antiferromagnetic (AFM) rhombohedral unit cell, which contains two formula units. Electron Bloch functions are obtained with the linearized-augmented-plane-wave method within both the local-spin density (LSD) and the LSD+U schemes. The thirteen uppermost occupied spin-up bands correspond in a pure ionic scheme to the five Mn $3d$ orbitals at the Mn_1 (spin-up) site and the four O $2s/2p$ orbitals at each of the O_1 and O_2 sites. Maximal localization identifies uniquely four Wannier functions for each O, which are trigonally distorted sp^3-like orbitals. They display a weak covalent bonding between O $2s/2p$ states and minority-spin d states of Mn_2, which is absent in a fully ionic picture. This bonding is the fingerprint of the interaction responsible for the AFM ordering, and its strength depends on the one-electron scheme being used. The five Mn Wannier functions are centered on the Mn_1 site, and are atomic orbitals modified by the crystal field. They are not uniquely defined by the criterion of maximal localization and we choose them as the linear combinations that diagonalize the r^2 operator, so that they display the D_{3d} symmetry of the Mn_1 site.

DOI: 10.1103/PhysRevB.65.184422 PACS number(s): 75.30.Et, 75.50.Ee, 71.15.Ap

I. INTRODUCTION

The mean-field one-particle description of the electronic struture of periodic crystalline solids is usually based on extended Bloch functions (BF's). Within the Born–von Kármán periodic boundary conditions, the cyclic translational subgroup, which commutes with the effective one-electron Hamiltonian, contains N translations by corresponding direct lattice vectors $\mathbf{R}$. This Abelian subgroup has N one–dimensional irreducible representations, which are labeled with wave vectors $\mathbf{k}$ within the first Brillouin zone (BZ). Therefore, extended Bloch states $\psi_{m\mathbf{k}}(\mathbf{r})$ in this description are classified with two quantum numbers, the band index m and the crystal momentum $\mathbf{k}$, and are obtained by diagonalization of the effective one–electron Hamiltonian. An alternative description can be derived in terms of localized Wannier functions[1] (WF's) $w_n(\mathbf{r}-\mathbf{R})$, which are defined in real space via a unitary transformation performed on the Bloch functions. They are also labeled with two quantum numbers, the orbital index n and the direct lattice vector $\mathbf{R}$, indicating the unit cell they belong to. In contrast to BF's, WF's are useful, for example, in visualizing chemical bonds or in describing the dielectric properties of nonmetallic materials. They can be considered as the generalization to solids of the concept of ''localized molecular orbitals'' for finite systems.[2] However, one major problem in practical calculations within this representation is the nonuniqueness of WF's, related to the phase arbitrariness of the BF's, and to the arbitrary unitary transformations that can be performed on the BF's at any given $\mathbf{k}$ point in the BZ. As demonstrated recently by Marzari and Vanderbilt,[3] this nonuniqueness can be resolved in principle by imposing the further condition of maximal localization. However, some residual arbitrariness remains, related to the choice of the localization criterion.

The late transition-metal (TM) monoxides MnO, FeO, CoO, and NiO challenge the theory of electronic states since several decades. These highly correlated materials feature a Mott insulator character, and the conventional local-spin-density (LSD) scheme[4] gets into difficulties with the localized TM d orbitals, predicting incorrectly in particular their spectral weight and their energy relative to O $2p$ states. All these oxides have the rocksalt structure in their paramagnetic phase, while below the Néel temperature T_N, a type II antiferromagnetic (AFM) ordering occurs.[5] The experimentally well-documented compound MnO, which is considered to be in the intermediate charge-transfer/Mott-Hubbard regime, is a particularly suitable case study, since the available theoretical schemes apply best to this material. Indeed, because of the exchange stabilization of its half-filled d shell, even LSD predicts its insulating character, although the corresponding energy gap and magnetic moment are much smaller than experimental data. Several electronic structure calculations have been performed for MnO, using traditional band-structure schemes, such as unrestricted Hartree-Fock[6] (UHF) and local-spin density (LSD), as well as more innovative approaches taking into account at various levels the large value of the on-site Coulomb repulsion for the metal $3d$ states, such as the SIC (Ref. 7) and the LSD+U (Ref. 8) methods, and the more recent GW model scheme.[9,10] Among the quantities calculated within the latter approach, special

attention has been devoted to the quasiparticle spectrum,[9] and recently to the zone-center optic phonon frequencies and the Born effective charge tensor.[6] Comparison with experimental data of the various physical quantities computed in the different schemes has demonstrated a monotonic trend with the separation energy between occupied and empty *d* bands, which is too small within LSD, too high within UHF, and has about the correct value within the *GW* model. This energy separation is strongly related to the on-site interaction *U*. The analysis of all these results has been performed in terms of the extended Bloch states.

On the other hand, no *ab initio* investigation exists of the electronic states in AFM MnO in terms of localized Wannier functions. Keeping in mind the inherent limitations of the mean-field one-particle approaches, it would be, however, instructive to materialize within the WF description how superexchange (which is responsible for AFM ordering) manifests itself in a first-principles one-electron picture. Furthermore, the maximal localization method of Marzari and Vanderbilt has been applied in the past to several periodic systems,[3,11,12] but not yet to a low (trigonal) symmetry solid such as AFM MnO, nor to a compound with a partially filled cation *d* shell.

Motivated by the reasons above, we present in this work an *ab initio* calculation of the maximally localized Wannier functions of AFM MnO corresponding to the uppermost occupied bands, using the all–electron, full–potential linearized–augmented–plane–wave (FLAPW) method.[13,14] Because the trends in the electronic properties from UHF to LSD are already known for this system, most of the computations have been performed for convenience within the latter scheme. To investigate the effects related to the on-site Coulomb interaction, we have also used the LSD+*U* method, implemented with the same FLAPW technical ingredients[15] used in the LSD computations.

The manuscript is organized as follows. In Sec. II we give technical details of the FLAPW implementation and structural information relevant to AFM MnO. The necessary ingredients of our WF calculations are then introduced. As we follow closely the formalism of Ref. 3, we will not describe in detail the method itself. A general result regarding maximal localization of *s*-*p* WF's is deferred to the Appendix. In Sec. III, we present and discuss the results of our maximally localized WF calculations. Finally, in Sec. IV we draw our conclusions.

II. METHOD

A. FLAPW calculations

All quantities presented and discussed in this paper have been computed using the semirelativistic FLAPW method,[13,14] expanded with local orbitals[16] (LO's) where appropriate. Inclusion of LO's in addition to the normal FLAPW basis enforces mutual state orthogonality and increases variational freedom. This allows us to treat the semicore Mn $3s,3p$ states together with the valence states, and helps in dealing with the linearization of Mn $3d$ and O $2s,2p$ states. Core states are calculated fully relativistically and self-consistently in the crystal potential. For the LSD calculations, the Hedin and Lundqvist exchange-correlation functional has been adopted. In the calculations performed within the LSD+*U* method, the values of the Hubbard and exchange constants, $U=6.9$ eV and $J=0.86$ eV, have been taken from Ref. 8. The atomic-sphere radii for Mn and O are chosen to be 2.0 and 1.8 a.u., respectively, and the FLAPW basis size is set to include all plane waves with energy up to 16.0 Ry. Four special points inside the irreducible wedge of the BZ were used for evaluating the charge density during self-consistency cycles.

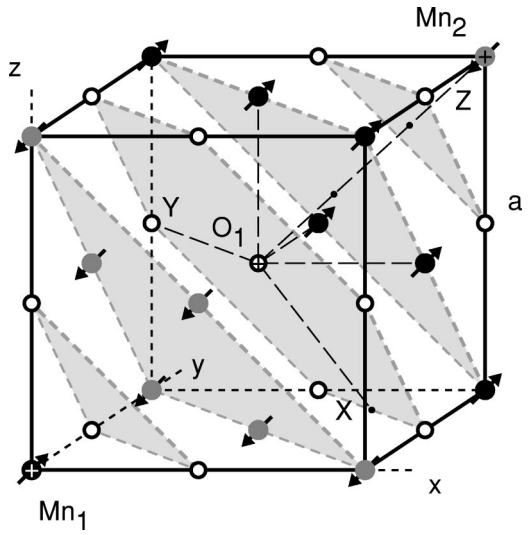

FIG. 1. Antiferromagnetic structure of MnO. Magnetic moments are arrayed in ferromagnetic sheets (shaded areas) parallel to (111) planes. Mn_1, Mn_2, and $O_{1,2}$ sites are given by large black, large gray, and small open circles, respectively. The trigonal coordinate axes are also indicated with long-dashed lines.

B. Structural details

AFM ordering occurs in MnO below $T_N=117$ K along any one of the $\langle 111\rangle$ directions. The transition is accompanied by a small crystallographic distortion that transforms the cubic structure into a rhombohedral one:[17] the 90° angle between the lattice vectors increases only by 0.624°. We have shown[6] earlier that the effect of this distortion on the calculated zone-center optic phonon frequencies and Born effective charge tensor is negligible compared to the anisotropy induced solely by the magnetic order. Therefore, throughout the present study we use the ionic positions of the perfect rocksalt chemical cell, with the experimental lattice constant value $a=4.435$ Å. In the AFM phase, the magnetic moments of MnO are arranged into ferromagnetic sheets which are parallel to (111), while the direction of magnetization in neighboring planes is reversed. The magnetic and crystalline structure of MnO is shown in Fig. 1. The rhombohedral magnetic cell, whose volume is twice that of the paramagnetic rocksalt one, corresponds to the space group D_{3d}^5 $(R\bar{3}m)$. Several choices for the primitive translation vectors are possible. However, in order to minimize discrete mesh effects in **k**-space integrations, and also for taking advantage of symmetry properties (see below), we

consider here the following primitive translation vectors (in the cubic coordinate system): $\mathbf{t}_1=a(1,\frac{1}{2},\frac{1}{2})$, $\mathbf{t}_2=a(\frac{1}{2},1,\frac{1}{2})$, and $\mathbf{t}_3=a(\frac{1}{2},\frac{1}{2},1)$. The two equivalent anions O_1 and O_2, whose site symmetry is C_{3v}, are located at positions $\pm a(\frac{1}{2},\frac{1}{2},\frac{1}{2})$, while the two nonequivalent cations Mn_1 (spin up) and Mn_2, whose site symmetry is D_{3d}, are at $(0,0,0)$ and $a(1,1,1)$. With our choice of origin on Mn_1, the two oxygen sites are therefore related by spatial inversion.

C. Maximally localized Wannier functions

We consider the general case of a *composite group* of energy bands labeled by their band index $m=1,2,\ldots,f$, and connected among themselves by degeneracies along high symmetry lines, but isolated from all other bands at lower and higher energy. The phase arbitrariness (gauge dependence) of each $|\psi_{m\mathbf{k}}\rangle$ with respect to the set of allowed $\mathbf{k}$ values propagates to the corresponding Wannier functions $|w_{n\mathbf{R}}\rangle$, labeled by $n=1,2,\ldots,f$ and lattice vectors $\mathbf{R}$. This resulting nonuniqueness manifests itself through an arbitrary unitary matrix $U^{(\mathbf{k})}_{mn}$ appearing in the most general transformation between BF's and WF's, which is given by

$$|w_{n\mathbf{R}}\rangle=\frac{V}{(2\pi)^3}\int_{\mathrm{BZ}}d\mathbf{k}e^{-i\mathbf{k}\cdot\mathbf{R}}\sum_m U^{(\mathbf{k})}_{mn}|\psi_{m\mathbf{k}}\rangle, \tag{1}$$

where V is the real-space primitive cell volume. A direct consequence of this arbitrariness is that linear combinations of the WF's in the set $\{|w_{n\mathbf{R}}\rangle\}$ also form a suitable basis.

The strategy of Ref. 3 is to pick out from this arbitrary choice of WF's the particular set that is maximally localized according to some criterion. Once this criterion has been chosen, and the composite group of bands specified, the search for the set of maximally localized WF's becomes a problem of functional minimization in the space of the matrices $U^{(\mathbf{k})}_{mn}$. The selected functional, which measures the sum of the quadratic spreads of the WF's probability density, is given by

$$\Omega=\sum_n\ [\langle r^2\rangle_n-\langle\mathbf{r}\rangle_n^2], \tag{2}$$

where $\langle\mathbf{r}\rangle_n=\langle w_{n\mathbf{0}}|\mathbf{r}|w_{n\mathbf{0}}\rangle=i[V/(2\pi)^3]\int_{\mathrm{BZ}}d\mathbf{k}\langle u_{n,\mathbf{k}}|\nabla_{\mathbf{k}}|u_{n,\mathbf{k}}\rangle$ and $\langle r^2\rangle_n=\langle w_{n\mathbf{0}}|r^2|w_{n\mathbf{0}}\rangle_n$. In these expressions, $u_{n,\mathbf{k}}(\mathbf{r})=e^{-i\mathbf{k}\cdot\mathbf{r}}\Sigma_m U^{(\mathbf{k})}_{mn}\psi_{m\mathbf{k}}(\mathbf{r})$ is a periodic function that can be obtained from the Bloch functions of the composite group of bands. Practically, one calculates the BF's on equispaced Monkhorst-Pack[18] meshes of $\mathbf{k}$ points in the unit cell $\overline{BZ}$ (whose volume is equal to the conventional BZ one), built on the reciprocal-lattice vectors. The grids have been offset in order to include Γ. With our chosen cell geometry of MnO, the reciprocal lattice vectors are $\mathbf{g}_1=(\pi/a)(3,-1,-1)$, $\mathbf{g}_2=(\pi/a)(-1,3,-1)$, and $\mathbf{g}_3=(\pi/a)(-1,-1,3)$. We then express the matrix elements of the gradient ∇_k appearing in the localization functional in terms of finite differences. As shown in Ref. 3, the only information needed is the overlap matrix $M^{(\mathbf{k},\mathbf{b})}_{nn'}=\langle u_{n\mathbf{k}}|u_{n',\mathbf{k}+\mathbf{b}}\rangle$, where $\mathbf{b}$ are vectors connecting each mesh point to its nearest neighbors. From these quantities, the gradient of the spread functional Ω with respect to an infinitesimal unitary transformation $\delta U^{(\mathbf{k})}_{mn}$ of the BF's can also be evaluated. Once this gradient is computed, the minimization can take place via a steepest-descent or conjugate-gradient algorithm.

It is important to stress that if the minimum of Ω is flat (as it will be shown to be the case for some of the MnO WF's), its precise location may be hindered by the various numerical approximations involved in the calculations. In this work, we have especially taken care of the following features, which clearly become irrelevant in the limit of a dense mesh ($N\to\infty$, $b\to 0$): (i) the regular mesh $\{\mathbf{k}\}_{\overline{\mathrm{BZ}}}$ has been chosen in order to have the lattice symmetry, i.e., it transforms into itself by application of the point group operations R of the crystal; (ii) the shell of $\mathbf{b}$ vectors used in the finite-difference formula for $\nabla_{\mathbf{k}}$ has been constructed on the 12 vectors of type $\{332\}$ and $\{1\bar{1}0\}$ (in internal units). They are the side midpoints of cubes that can be built on particular points of the rhombohedral mesh, and this set of 12 points is therefore compatible with the highest possible symmetry.

Finally, and following the procedure described in Eqs. (62)–(64) of Ref. 3, we start the minimization procedure by constructing a set of ''trial functions'' in the unit cell, which are an initial guess of the final WF's. We use Gaussians centered on atomic sites and modulated by an appropriate combination of spherical harmonics, with a rms width value such that the Gaussian is negligible outside the corresponding atomic sphere. A unitary rotation among the initial BF's is then performed in order to maximize their projection on the trial functions.

It has been shown[19] that Wannier functions can be chosen with well-defined symmetry properties, and forming (generally reducible) representations of the crystal point group. In order to investigate the nature and possible reductions of these representations in the case of MnO, and also to be in the position to use group–theory methods for further analysis, we need to calculate the representation matrix elements $\langle w_{n'\mathbf{0}}|P_R|w_{n\mathbf{0}}\rangle$, where P_R is the transformation operator corresponding to the operation R of the point group, and the WF's are in the central cell. For simplicity, we restrict the formalism to symmorphic space groups (which is actually the case for D^5_{3d}). Using Eq. (1) with the $\mathbf{k}$-point discretization and $\mathbf{R}=\mathbf{0}$, we have for the rotated Wannier function

$$P_R|w_{n\mathbf{0}}\rangle=\frac{1}{N}\sum_{\mathbf{k}\in\overline{\mathrm{BZ}}}\sum_m U^{(\mathbf{k})}_{mn}P_R|\psi_{m\mathbf{k}}\rangle, \tag{3}$$

and, with the ''periodic gauge'' condition, $\psi_{mR\mathbf{k}}(\mathbf{r})=\psi_{mR\mathbf{k}+\mathbf{G}_{\mathbf{k}}}(\mathbf{r})$,

$$\begin{aligned}\langle w_{n'\mathbf{0}}|P_R|w_{n\mathbf{0}}\rangle_{NV}&=\frac{1}{N^2}\sum_{\mathbf{k},\mathbf{k}'\in\overline{\mathrm{BZ}}}\sum_{m,m'}U^{*(\mathbf{k}')}_{m'n'}U^{(\mathbf{k})}_{mn}\langle\psi_{m'\mathbf{k}'}|P_R|\psi_{m\mathbf{k}}\rangle_{NV}\\&=\frac{1}{N}\sum_{\mathbf{k}\in\overline{BZ}}\sum_{m,m'}U^{*(R\mathbf{k}+\mathbf{G}_{\mathbf{k}})}_{m'n'}U^{(\mathbf{k})}_{mn}\langle\psi_{m'R\mathbf{k}+\mathbf{G}_{\mathbf{k}}}|P_R|\psi_{m\mathbf{k}}\rangle_V.\end{aligned} \tag{4}$$

TABLE I. Classification of *s*, *p*, and *d* atomic orbitals according to the irreducible representations of O_h together with their reduction into irreducible representations of D_{3d} and C_{3v}, and the corresponding basis. Bethe notation (Ref. 20) is used. The cubic and trigonal coordinate systems are denoted by x,y,z and X,Y,Z, respectively.

O_h irreducible representations		Reduction into D_{3d} (C_{3v}) irreducible representations and basis	
Γ_1^+	s	$\Gamma_1^+(\Gamma_1)$	s
	p_x	$\Gamma_2^-(\Gamma_1)$	$(p_x+p_y+p_z)/\sqrt{3}\equiv p_Z$
Γ_4^-	p_y		$(p_x+p_y-2p_z)/\sqrt{6}\equiv p_X$
	p_z	$\Gamma_3^-(\Gamma_3)$	$(p_x-p_y)/\sqrt{2}\equiv p_Y$
	$d_{x^2-y^2}$		$d_{x^2-y^2}$
Γ_3^+	d_{z^2}	$\Gamma_3^+(\Gamma_3)$	d_{z^2}
	d_{xy}	$\Gamma_1^+(\Gamma_1)$	$(d_{yz}+d_{zx}+d_{xy})/\sqrt{3}\equiv d_{Z^2}$
Γ_5^+	d_{yz}		$(d_{yz}+d_{zx}-2d_{xy})/\sqrt{6}$
	d_{zx}	$\Gamma_3^+(\Gamma_3)$	$(d_{yz}-d_{zx})/\sqrt{2}$

The last bra-ket is trivial only in the case of nondegenerate BF's. In the general case, on the other hand, we have

$$P_R\psi_{m\mathbf{k}}(\mathbf{r})=\psi_{m\mathbf{k}}(R^{-1}\mathbf{r})=\sum_{m'} D_{m'm}(R,\mathbf{k})\psi_{m'R\mathbf{k}}(\mathbf{r}), \quad (5)$$

where $D_{m'm}(R,\mathbf{k})$ is a unitary transformation associated with the symmetry operation R, and the summation is over states degenerate with $\psi_{m'R\mathbf{k}}(\mathbf{r})$. If this latter state is nondegenerate, $D_{m'm}(R,\mathbf{k})=\delta_{m'm}$, and Eq. (5) becomes the usual formula. We note that the above formulas allow us to decompose $|w_{n\mathbf{0}}\rangle$ into a linear combination of basis functions transforming according to the relevant irreducible representations of the point group.

III. RESULTS

For our Wannier-function description of the electron states in AFM MnO, we have considered as a single composite group the topmost thirteen valence bands (O $2s$, O $2p$, Mn $3d$). In this way, the corresponding Wannier functions display the highest localization, and therefore can be considered as the ''elementary building blocks'' of the occupied electron states. As it is convenient to interpret some of our results in terms of combinations of atomic orbitals, we give in Table I the relevant O_h representations corresponding to *s*, *p*, and *d* orbitals and their reduction into irreducible representations of D_{3d} and C_{3v}, together with their corresponding basis. Cartesian coordinates in the parent cubic reference system are written using *x*, *y*, and *z* symbols, while *X*, *Y*, and *Z* correspond to the trigonal reference system (*Z* axis along the cubic [111] direction). Throughout this work, we use the Bethe notation for the irreducible representations.[20]

We have first studied the convergence of the spread functional Ω in terms of the mesh density, using a sampling of the Brillouin zone $\overline{BZ}$ defined by the Monkhorst-Pack meshes $\nu\times\nu\times\nu$ with $\nu=2$, 4, 6, and 8. Analysis has been done on the various terms of the localization functional Ω discussed in Ref. 3. We found that a satisfactory level of convergence is achieved using the $6\times6\times6$ mesh, which represents a good compromise between accuracy and computer burden. Also, such a mesh is large enough to prevent difficulties related to finite grids and the occurrence of periodic WF replica. The $6\times6\times6$ sampling has been retained throughout this work.

TABLE II. Center and spread of the four Wannier functions for the O_1 site corresponding to the uppermost LSD spin-up valence bands of MnO. Center components $\overline{r_x}$, $\overline{r_y}$, and $\overline{r_z}$ are given with respect to the atomic site in the cubic reference system. The sum of WF centers and the total spread are also displayed. Values in parentheses correspond to the LSD+U scheme. Considering the C_{3v} symmetry of the O_1 site, WF 1 belongs to Γ_1 while WF's 2, 3, and 4 are equivalent to each other. WF's 5–8 for the O_2 site have the same Ω and opposite $\overline{\mathbf{r}}$.

WF	$\overline{r_x}$ (Å)	$\overline{r_y}$ (Å)	$\overline{r_z}$ (Å)	Ω (Å^2)
1	0.174	0.174	0.174	0.751
	(0.186)	(0.186)	(0.186)	(0.686)
2	−0.387	0.036	0.036	0.773
	(−0.366)	(0.049)	(0.049)	(0.704)
3	0.036	−0.387	0.036	0.773
	(0.049)	(−0.366)	(0.049)	(0.704)
4	0.036	0.036	−0.387	0.773
	(0.049)	(0.049)	(−0.366)	(0.704)
Total	−0.141	−0.141	−0.141	3.069
	(−0.082)	(−0.082)	(−0.082)	(2.797)

The minimization of the localization functional, which determines the unitary matrix $U_{mn}^{(\mathbf{k})}$, has been performed using a mixed strategy: a simple fixed-step steepest-descent procedure is used during the first iterations, followed by several iterations with a conjugate–gradient procedure that is reset to steepest descent every 100 iterations. Because of the delicate convergence of the Mn WF's, and in order to be on the safe side, we used a very large number (40 000–80 000) of iterations.

Several choices of trial orbitals have been tested to initialize efficiently the minimization procedure. In particular (see Sec. II C), we have considered the following sets of initial trial orbitals: (i) Gaussians times real combinations of spherical harmonics *s*, p_x, p_y, and p_z on the O_1 and O_2 oxygen sites, and d_{z^2}, $d_{x^2-y^2}$, d_{xy}, d_{yz}, and d_{zx} on the manganese Mn_1 site. These real harmonics, reported in Table I, form the basis of reducible representations of C_{3v} (O site) and of D_{3d} (Mn_1 site), and are oriented along cubic axes. (ii) The same centers as above, but with Gaussians modulated by spherical harmonics combinations *s*, p_X, p_Y, p_Z, and d_{Z^2}, $d_{X^2-Y^2}$, d_{XY}, d_{YZ}, and d_{ZX}, i.e., basis functions of the irreducible representations of C_{3v} and D_{3d}. (iii) Combinations of the two above possibilities. All these sets of initial trial orbitals eventually lead, at convergence, to the same WF's, which are real, in agreement with the discussion in Ref. 3. However, the set (i) corresponds to a much faster convergence than the other choices. The reason is directly related to the shape and orientation of the final O $2s/2p$ WF's, and this point will be discussed further below.

TABLE III. The spreads (in Å^2) of the five Wannier functions (9–13) centered at the origin (Mn_1 site) corresponding to the uppermost LSD and LSD $+U$ spin–up valence bands of MnO. Total spreads are also indicated. The meaning of s-LSD and s-LSD$+U$ is explained in the text.

	9	10	11	12	13	Tot. (9–13)
LSD	0.6220	0.6218	0.6497	0.6493	0.6493	3.193
s–LSD	0.5950	0.5950	0.6248	0.6899	0.6899	3.194
s-LSD$+U$	0.4713	0.4713	0.5133	0.5163	0.5163	2.488

We give in Table II the converged Wannier centers and spreads corresponding to the four oxygen WF's at the O_1 site for the spin-up channel. $\bar{r}_x$, $\bar{r}_y$, and $\bar{r}_z$ are the components of the Wannier center position with respect to the corresponding atomic site. We give also the total spread Ω of these four WF's, and the sum of the corresponding centers whose interpretation will be discussed below. WF's related to the O_2 site have the same Ω and opposite $\bar{\mathbf{r}}$. The spreads corresponding to the five LSD WF's (9–13) at the Mn_1 site are given in the first line of Table III. By symmetry, these WF's are centered on the Mn_1 site (origin). Because the two oxygen sites are equivalent, corresponding results for the spin-down channel can be simply obtained by reversing Mn_1 and Mn_2. The total spread (sum of the 13 individual spreads) is 9.332 Å^2. We note also that the sum of centers has all Cartesian components equal to zero. Indeed, this quantity represents the electronic polarization (modulo a lattice vector) corresponding to valence states, and its zero value is compatible with the fact that the system is centrosymmetric. In order to analyze in detail Table II, it is useful to construct the matrix elements of the representation of the symmetry operations of the D_{3d} point group on the basis of the 13 Wannier functions. This is done by using Eq. (4). First, we have verified by constructing the multiplication table that these 12 matrices form indeed a representation of D_{3d}. For nontrivial operations of the point group D_{3d}, they display the following structure: (i) There is an 8×8 block corresponding to O $2s/2p$ Wannier functions. Each line of this block consists of zeros, except for one element that is equal to 1. Because the origin is on the Mn_1 site, the operations of D_{3d} are simply transforming all WF's on *both* O sites into each other. (ii) There is a 5×5 block corresponding to Mn_1 $3d$ Wannier functions. This block does not display a well-defined structure, and in general all its elements are nonzero. (iii) The two off-diagonal blocks (connecting O $2s/2p$ and Mn_1 $3d$ WF's) have all their elements equal to zero, at an accuracy better than 10^{-7}. Therefore, the 13×13 representation is block-diagonal, and in particular the 5×5 Mn_1 $3d$ block makes a (reducible) representation by itself.

We discuss first the O $2s/2p$ Wannier functions. The two nonequivalent WF's corresponding to site O_1 are shown in Fig. 2, with a viewpoint which is about the same as in Fig. 1. The equivalent WF's corresponding to site O_2 can simply be obtained by inversion symmetry with respect to the origin. In the absence of discrimination between Mn_1 and Mn_2 sites, the oxygen site would have cubic (O_h) symmetry, and the four converged WF's originating from s and p states on the same O_1 site would be sp^3 hybrids. This is a general result, which is demonstrated in the Appendix: from localized atom-centered s-p orbitals, the maximal localization algorithm always favors sp^3-like Wannier functions, provided that the symmetry is cubic or higher. This situation occurs, e.g., in a hypothetical ferromagnetic (FM) MnO crystal, which will be briefly described later. In AFM MnO, Mn_1 and Mn_2 sites are nonequivalent, so that the symmetry of the oxygen site is reduced to C_{3v}. However, reminiscence of the sp^3 hybrids persists: disregarding for the moment the d admixture, we see in panel (a) of Fig. 2 that the WF 1, with Γ_1 symmetry, displays clearly the shape of a nonsymmetric p_z orbital, with its center shifted from the atomic site along the [111] direction (p_z-s mixing), as also indicated in Table II. The three other WF's are equivalent to each other under the operations of C_{3v} (they have the same spread), and their centers are located much closer to the cubic axes than to the diagonals. This can be explained by considering the interaction with the $3d$ orbitals of Mn_2: all these WF's display a substantial bonding $3d$ contribution from the three neighboring unoccupied Mn_2 sites. As the first-neighbor shell of Mn sites is an octahedron centered on each O, the above interaction favors the orientation of the equivalent WF's 2, 3, and 4 along cubic axes. We display in panel (b) of Fig. 2 the WF 2 whose center is close to the [100] axis. The sum of WF centers given in Table II is a measure of the trigonal distortion of the sp^3-like orbitals, since it would be vanishing in a perfect cubic environment. This configuration of the converged WF's justifies also our choice of trial orbitals: p_x, p_y, and p_z orbitals are already good guesses of final WF's 2, 3, and 4. During the iterations, most of the effort is devoted to building up WF 1 (the p_z–s hybrid oriented along [111]). We note also in Fig. 2 small features on the neighboring Mn_1 sites. They correspond to a weak bonding contribution from unoccupied states on these sites.

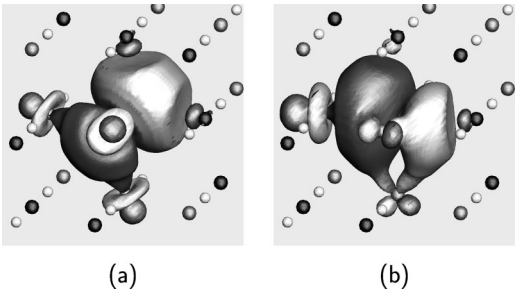

FIG. 2. LSD Wannier functions of AFM MnO corresponding to the whole spin-up valence–band complex (13 bands). (a) The $2s/2p$ WF of O_1 with center along the [111] direction; (b) one of the three equivalent O_1 WF's, with center close to the [100] axis. The Mn_1, Mn_2, and $O_{1,2}$ sites are denoted by large black, large gray, and small white spheres, respectively. Light gray and dark gray colors indicate the positive and negative amplitudes of the WF contours.

We consider next the five Mn_1 $3d$ Wannier functions. They are exactly centered at the Mn_1 site and their spreads do not display any well-defined symmetry. When convergence of O $2s/2p$ Wannier functions is practically achieved, further iterations of the localization process have the only

effect of modifying slightly (essentially by amounts comparable to the numerical noise) the individual spreads of the five Mn_1 $3d$ WF's, while their total spread remains unchanged. These five WF's are not uniquely defined by the criterion of maximal localization. In fact, any set of WF's obtained by applying a unitary transformation to the original set will in general have different individual spreads, but the same value of the total spread. Since it is advisable that the final WF's display explicitly as much symmetry as possible, we exploit this nonuniqueness and perform a symmetry reduction of the fivefold representation of the Mn_1 $3d$ WF's, which decomposes into $\Gamma_1^+ + 2\Gamma_3^+$ according to D_{3d} symmetry.

We note that the Hermitian operator r^2, which appears in the localization functional Eq. (2), has the full rotational symmetry, and therefore its matrix representation $\langle r^2 \rangle_{n'n} = \langle w_{n'\mathbf{0}} | r^2 | w_{n\mathbf{0}} \rangle$ belongs to the Γ_1^+ representation of D_{3d}. These matrix elements can be calculated through a simple generalization of Eq. (23) of Ref. 3, and are given by

$$\langle w_{n'\mathbf{0}} | r^2 | w_{n\mathbf{0}} \rangle = \frac{1}{N} \sum_{\mathbf{k},\mathbf{b}} w_b [2\delta_{n'n} - M_{n'n}^{(\mathbf{k},\mathbf{b})} - M_{nn'}^{(\mathbf{k},\mathbf{b})*}]. \tag{6}$$

We choose the five new WF's as the linear combinations of the original set that diagonalize the r^2 matrix, Eq. (6). We get in this way an extra unitary transformation that allows us to update the matrices $U^{(\mathbf{k})}$. The resulting WF's, which display the expected $(\Gamma_1^+ + 2\Gamma_3^+)$ symmetry, are indicated with the header "s-LSD" in Table III, and are shown in Fig. 3. We note that an arbitrariness (up to a 2×2 unitary transformation) remains in the definition of the partners in the two Γ_3^+ representations. Figure 3 shows that the WF's 9–13 are essentially atomic orbitals modified by the D_{3d} crystal field.

The picture above depicting the whole set of WF's in AFM MnO has been confirmed by similar calculations performed for a hypothetical FM MnO crystal. In this case, the symmetry is cubic (space group O_h^5), and the majority-spin channel contains 18 valence states (O $2s$, O $2p$, and Mn $3d$), while the minority-spin channel has 8 valence states (O $2s$, O $2p$). As in AFM MnO, the Mn $3d$ WF's are found to be essentially atomic orbitals. By contrast, the O $2s/2p$ WF's in both chanels are here undistorted sp^3 hybrids (see Appendix). In the minority-spin channel, *both* lobes of each hybrid display a substantial bonding $3d$ contribution from the three neighboring unoccupied Mn sites, while these features are absent in the majority-spin channel (occupied Mn sites). The sp^3-like oxygen WF's, with the center along the [111] direction, are shown in Fig. 4 for both spin channels.

The covalent interaction in AFM MnO between O and Mn_2 $3d$ orbitals, clearly singled out in Fig. 2 for the case of the spin-up channel (we remind the reader that corresponding results for the spin-down case are obtained by reversing Mn_1 and Mn_2), is the fingerprint of superexchange in a one-electron picture. The superexchange mechanism results in fact from indirect many-body interactions, involving metal atoms (here Mn_1 and Mn_2) with an intervening oxygen. The shared covalency of nearest-neighbor pairs of magnetic ions leads to an antiferromagnetic alignment of their moments. As

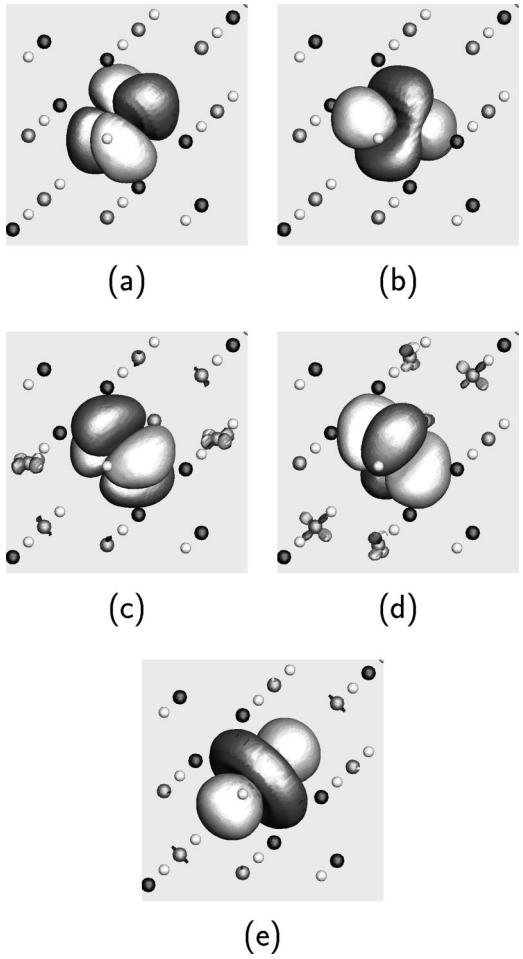

FIG. 3. Same as Fig. 2, but for the five Mn_1 $3d$ WF's within LSD, after diagonalization of $\langle r^2 \rangle_{n'n}$. The WF's (a) and (b), as well as (c) and (d), are partners of a Γ_3^+ representation of D_{3d}, while (e) belongs to Γ_1^+.

a matter of fact, supposing, e.g., a spin-up WF on the Mn_1 site, the neighboring Mn WF has the choice between two spin orientations, corresponding to a FM or an AFM ordering. The FM choice will be energetically less favorable, due to the required orthogonalization to the Mn_1 WF, while in the AFM alignment, the spin part of the wave function accounts for this necessary orthogonalization. The textbook explanation above of AFM ordering can be discussed in light of our

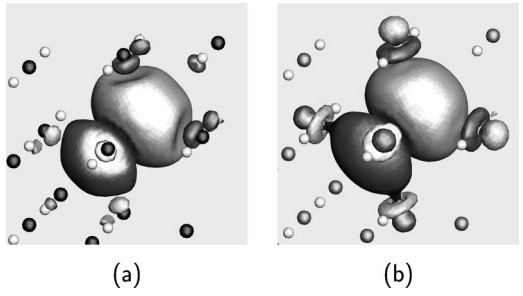

FIG. 4. LSD Wannier functions of FM MnO. The sp^3-like O WF with the center along the [111] direction for (a) majority and (b) minority spin. Notations are the same as in Fig. 2.

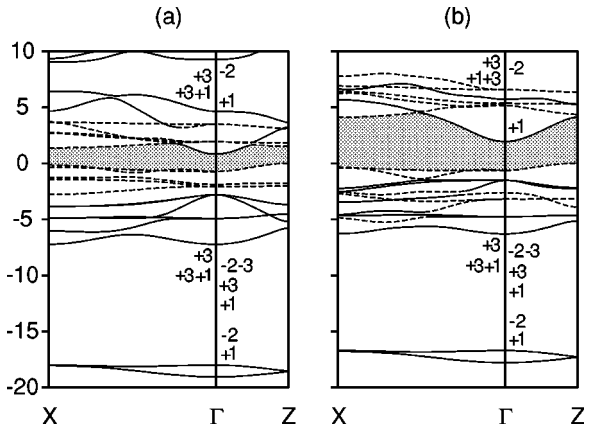

FIG. 5. Energy bands of antiferromagnetic MnO calculated along the X-Γ-Z lines of the rhombohedral magnetic zone using (a) the local-spin-density approximation and (b) the LSD+U scheme. Shaded areas correspond to the fundamental gap. Irreducible representations at Γ (Bethe notation) are also given on the left and right of the energy axis, for states of primary Mn and O origin, respectively. Bands corresponding to states with high probability in the Mn atomic spheres are drawn with dashed lines.

calculations, showing a real-space representation of the WF's for an AFM system. The maximally localized WF's bring out the relevant physical information, namely the covalent interaction with empty Mn $3d$ states. We also notice that the FM alignment, on the other hand, is favored by kinetic energy. This can be seen in Figs. 2 and 4 from the larger number of covalent interactions (6 instead of 3 in AFM case) associated with the O sp^3-like WF's, which leads eventually to a broader bandwidth.

It is useful at this point to contrast this rather simple one-electron picture of AFM MnO, obtained in real space using the localized Wannier-function description, with the more entangled picture based on the energy band structure of the extended Bloch-function description. For this purpose, we show in the left panel of Fig. 5 the spin-up band structure of MnO along the X-Γ-Z directions, calculated within the LSD scheme. Starting from the lowest energies, we find first a Γ_1^+ and a Γ_2^- state at $\mathbf{k}=\mathbf{0}$. They arise from Γ_1 O $2s$ orbitals on the two O sites (related by inversion symmetry), forming symmetric (Γ_1^+) and antisymmetric (Γ_2^-) combinations, respectively. The primary origin of the next composite group of 6 bands is O $2p$ triplets on the two O sites, which are split into a Γ_1 singlet and a Γ_3 doublet by trigonal C_{3v} site symmetry. They lead to one set of symmetric combinations (Γ_1^+, Γ_3^+), and one set of antisymmetric combinations (Γ_2^-, Γ_3^-) between the two sites. Next, the occupied t_{2g} orbitals of the Mn_1 atom are split at Γ into a doublet plus a singlet (Γ_3^+, Γ_1^+), while the e_g orbitals remain a doublet (Γ_3^+). These Mn_1 $3d$ orbitals give rise to the uppermost occupied composite group of five bands. Clearly, states of the Mn_1 $3d$ and O $2p$ complexes that belong to the same Γ_1^+ (or Γ_3^+) representation interact with each other, so that eventually both sets $\Gamma_1^+(Mn_1\ d)$, $\Gamma_1^+(O\ p)$ and $\Gamma_3^+(Mn_1\ d)$, $\Gamma_3^+(O\ p)$ consist of bonding and antibonding partners of Mn_1 $3d$/O $2p$ hybrids. A mirror picture (relative to Fermi energy) of the description above applies to the conduction bands that originate from the Mn_2 $3d$ orbitals, if we exclude the lowest conduction band at Γ, which is free-electron-like, has mostly Mn $4s$/O $3s$ character, and is not relevant to the present discussion. The description above would leave completely empty the spin-up $3d$ states of the Mn_2 atom. However, a covalent interaction (clearly depicted in Fig. 2 within the Wannier-function description) between O $2p$ and the unoccupied Mn_2 $3d$ states takes place, and some amount of spin-up charge appears at the Mn_2 sites, which would be totally empty in a completely ionic picture. For instance, the highest antibonding Γ_3^+ valence state at Γ has 60% d occupancy in the Mn_1 sphere, 7% p occupancy in each of the two O spheres, and 14% d occupancy in the Mn_2 sphere.

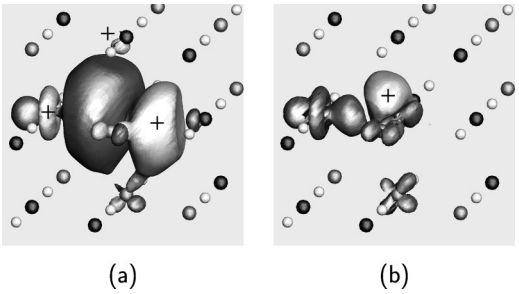

FIG. 6. (a) The $2s/2p$ WF of O_1 as in Fig. 2(b), but calculated within the LSD+U scheme; (b) charge-density difference (LSD +U minus LSD) corresponding to the WF of panel (a). Light gray (a "+" sign has been added for clarity) and dark gray colors indicate positive and negative contour values, respectively.

With the above results in mind, it is instructive to investigate WF's within other one-electron schemes, leading to different degrees of wave-function localization, covalent interaction, and magnetic moments. Data corresponding to the LSD+U scheme are presented in Tables II and III for the spin−up channel. Values for the Mn_1 $3d$ WF's are those obtained after diagonalization of $\langle r^2\rangle_{n'n}$. All individual spreads, as well as the total spread (whose value is 8.083 Å^2), are smaller than those in the LSD case: the O $2s/2p$ and Mn $3d$ Wannier functions are more localized by 9% and 22%, respectively, and this is consistent with the narrower valence bandwidth. This property appears also in Fig. 6, where we show the LSD + U result for the WF 2 derived from O $2s/2p$ states. This LSD+U orbital is similar to the corresponding one calculated within LSD, and displayed in Fig. 2(b). The most noticeable difference appears in the weaker covalent interaction between O and the Mn_2 $3d$ orbitals. This is clearly visible in the right panel of Fig. 6, where we display the d-like differential charge density ($\rho_{\mathrm{LSD+U}}-\rho_{\mathrm{LSD}}$) associated with this particular oxygen WF. The five Mn_1 $3d$ WF's, obtained within LSD+U, are very similar to the LSD ones, and are essentially atomic orbitals modified by the crystal field.

The more localized character of all WF's within the LSD+U scheme, together with the weaker covalent interaction between O and Mn_2 $3d$ orbitals, is the fingerprint in the Wannier-function description of the larger on-site interaction U of cation $3d$ states. It is worth realizing that this simple trend is more easily detectable in terms of Wannier functions

than Bloch functions. To this end, we show in the right panel of Fig. 5 the LSD + U band structure of MnO. It differs in several respects from the LSD one. The energy gap (2.0 eV), though still smaller than the experimental one (3.8–4.2 eV), is closer to it than the LSD value (0.8 eV). The energy separation between occupied and empty d states, which is due to the on-site interaction U between cation $3d$ states, has also increased. Furthermore, the three Mn_1 $3d$ bands corresponding to the lower Γ_3^+ and Γ_1^+ states (t_{2g}) no longer form a composite group of bands by themselves, but rather mix with the O $2p$ complex. This results in a narrowing of the valence-band width (6.3 eV against 7.2 eV in LSD).

The distinct features of the WF's computed within LSD and LSD+U can be used for discussing the behavior of the Born dynamical charge tensor Z^* within these different many-body approximations. In fact, as Z^* can be defined in terms of the relative displacement of WF centers,[21] it carries along relevant information. In particular, a p-d interaction between valence and conduction states in mixed ionic-covalent materials[22] leads to anomalous Z^*, while atomiclike occupied WF's correspond to a nominal value. Therefore in MnO, one expects smaller $|Z^*|$ (i.e., closer to 2, its nominal value) within the LSD+U scheme, to which correspond more localized WF's than within LSD. We performed the calculation of the [111] component of this tensor, using the WF description, and obtained within LSD the value $|Z_{\|}^*| = 2.36$, which is consistent with the one obtained previously[6] using the Berry phase approach. The LSD+U scheme, on the other hand, gives as expected a smaller value $|Z_{\|}^*| = 2.26$. These results relate the behavior of two important physical quantities (the superexchange energy and Z^*) to the same information contained in the AFM MnO WF's, namely, the magnitude of their amplitudes on unoccupied Mn_2 sites in the different approximations.

IV. CONCLUSION

We have used the maximum localization criterion for constructing Wannier functions of AFM MnO within both LSD and LSD+U schemes. This is the first application of the method to a magnetic low-symmetry system, with a partially filled d band. The LSD+U approach has been considered here, as it improves the LSD description of the ground-state properties of strongly correlated materials. The Wannier-function description, which can be viewed as a generalization to extended systems of the localized molecular-orbital description of molecules, provides in the case of MnO a simple picture complementary to the Bloch-function one. We obtain two distinct groups of WF's: (i) the five Mn $3d$ WF's centered on the Mn_1 site, which are atomic orbitals modified by the crystal field; (ii) the four trigonally distorted sp^3 WF's associated with each of the O_1 and O_2 sites, which are not centered on these sites. The latter display a substantial covalent bonding with $3d$ states on Mn_2 sites, which is consistent with the AFM ordering of this material. Concerning the Mn WF's, they are not uniquely defined by the criterion of maximal localization. We have exploited this feature to obtain symmetrized maximally localized WF's. We impose this further condition by diagonalization of the r^2 operator.

ACKNOWLEDGMENTS

It is a pleasure to acknowledge stimulating discussions with D. Vanderbilt. We would like to thank N. Bernstein for providing us with his graphics program ''dan.'' This work was supported by the Swiss National Science Foundation (Grant No. 20–59121.99).

APPENDIX: MAXIMALLY LOCALIZED WANNIER FUNCTIONS FROM ONE s-LIKE AND THREE p-LIKE ORBITALS FOR CUBIC SITE SYMMETRY

We consider the four-dimensional Hilbert space $\mathcal{H}_4$ spanned by four orthonormal localized basis functions $|\phi_1\rangle$, $|\phi_2\rangle$, $|\phi_3\rangle$, and $|\phi_4\rangle$, centered on a given site (taken here as the origin) with cubic point-group symmetry (T, T_h, O, T_d, or O_h). $|\phi_1\rangle$ is the basis function of a representation Γ_1 (for T, O, and T_d) or Γ_1^+ (for T_h and O_h). $|\phi_2\rangle$, $|\phi_3\rangle$, and $|\phi_4\rangle$ are the basis functions of a threefold representation Γ_4 (for T and O), Γ_5 (T_d), Γ_4^+ (T_h), or Γ_4^- (O_h). More precisely, $|\phi_2\rangle = |\phi_x\rangle \in x$ row of the threefold representation, and $|\phi_3\rangle = C_3^{-1}|\phi_x\rangle$, $|\phi_4\rangle = C_3|\phi_x\rangle$, where C_3 is the rotation by $2\pi/3$ around the [111] axis. We consider real $|\phi_i\rangle$ functions, as the maximally localized WF's turn out to be real, apart from an arbitrary overall phase factor.[3] Finally, we suppose that the $|\phi_i\rangle$ ($i=1,\ldots,4$) are sufficiently localized so that $\langle\phi_i|\mathbf{r}|\phi_j\rangle$ and $\langle\phi_i|r^2|\phi_j\rangle$ exist and are finite.

We demonstrate below that minimizing within $\mathcal{H}_4$ the localization functional, Eq. (2), leads to sp^3-like Wannier functions, as opposed to the original atomiclike $|\phi_i\rangle$ functions. The solution is unique and corresponds to one of the two tetrahedra defined by the cubic point-symmetry group if the latter is T or T_d. For the higher symmetry groups T_h, O, and O_h, maximal localization leads to an infinity of sp^3-like solutions constructed from $|\phi_1\rangle$ and unitary transformed threefold functions $|\phi_2\rangle$, $|\phi_3\rangle$, $|\phi_4\rangle$ according to any of the 3×3 orthogonal matrices $\mathbf{D}^{(1)}(\alpha,\beta,\gamma)$ representing a rotation of the Cartesian coordinates of a vector.

As the operator r^2 belongs to the identity representation, it is diagonal in the $|\phi_i\rangle$ basis, and we have

$$\langle\phi_i|r^2|\phi_i\rangle = (\Omega_s \quad \Omega_p \quad \Omega_p \quad \Omega_p), \tag{A1}$$

where cubic symmetry has been taken into account. Similarly, writing $\mathbf{r} = x\mathbf{i} + y\mathbf{j} + z\mathbf{k}$ and using projection operators, we find after some algebra

$$\langle\phi_i|\mathbf{r}|\phi_j\rangle = \begin{pmatrix} 0 & \lambda\mathbf{i} & \lambda\mathbf{j} & \lambda\mathbf{k} \\ \lambda\mathbf{i} & 0 & \delta\mathbf{k} & \delta\mathbf{j} \\ \lambda\mathbf{j} & \delta\mathbf{k} & 0 & \delta\mathbf{i} \\ \lambda\mathbf{k} & \delta\mathbf{j} & \delta\mathbf{i} & 0 \end{pmatrix}, \tag{A2}$$

with $\lambda = \langle\phi_s|\xi|\phi_\xi\rangle$, where $\xi = x,y,z$, and $\delta = \langle\phi_x|y|\phi_z\rangle = \langle\phi_y|z|\phi_x\rangle = \langle\phi_z|x|\phi_y\rangle$. The phase arbitrariness of the orbitals allows us to set $\lambda \geqslant 0$. We note that symmetry requires $\delta = 0$ in the case of T_h, O, or O_h. The total spread of the original atomiclike $|\phi_i\rangle$ functions is

$$\Omega_\phi = \sum_i \left[\langle \phi_i | r^2 | \phi_i \rangle - |\langle \phi_i | \mathbf{r} | \phi_i \rangle|^2\right] = \Omega_s + 3\Omega_p . \tag{A3}$$

We consider now the four orbitals $|\psi_i\rangle$ obtained from the $|\phi_j\rangle$ by a general orthogonal transformation O, given explicitly by

$$|\psi_i\rangle = \sum_j O_{ij} |\phi_j\rangle \quad (i,j=1,\ldots,4). \tag{A4}$$

There are 6 independent matrix elements, and 10 orthonormality conditions for columns or rows. Using Eqs. (A1) and (A4) and the orthonormality conditions, we obtain

$$\begin{aligned}\sum_i \langle \psi_i | r^2 | \psi_i \rangle &= \sum_i \left[O_{i1}^2 \Omega_s + (O_{i2}^2 + O_{i3}^2 + O_{i4}^2)\Omega_p\right] \\ &= \sum_i \left[O_{i1}^2 \Omega_s + \Omega_p (1 - O_{i1}^2)\right] = \Omega_s + 3\Omega_p ,\end{aligned} \tag{A5}$$

which verifies the trace invariance property of Eq. (A1) under orthogonal transformations, and gives for the total spread Ω_ψ of the functions defined by (A4) the inequality

$$\begin{aligned}\Omega_\psi &= \sum_i \langle \psi_i | r^2 | \psi_i \rangle - \sum_i |\langle \psi_i | \mathbf{r} | \psi_i \rangle|^2 \\ &= \Omega_s + 3\Omega_p - \sum_i |\langle \psi_i | \mathbf{r} | \psi_i \rangle|^2 \\ &\leqslant \Omega_s + 3\Omega_p = \Omega_\phi .\end{aligned} \tag{A6}$$

Therefore, the atomiclike $|\phi_i\rangle$ functions correspond to the maximum value of the spread, and the problem of the total spread minimization reduces to minimizing the second term $-\Sigma_i |\langle \psi_i | \mathbf{r} | \psi_i \rangle|^2$ of the localization functional, which can be evaluated using Eqs. (A2) and (A4).

We consider next the two particular orthogonal transformations $\tilde{O}$ and $\tilde{O}'$ of the $|\phi_i\rangle$ corresponding to the two possible choices for the four sp^3 hybrid orbitals $|\tilde{\psi}_i\rangle$ and $|\tilde{\psi}'_i\rangle$ (written together below $|\tilde{\psi}_i^{(\prime)}\rangle$), and given explicitly by

$$\begin{aligned}|\tilde{\psi}_{111}^{(\prime)}\rangle &= \frac{1}{2}(|\phi_1\rangle \pm |\phi_2\rangle \pm |\phi_3\rangle \pm |\phi_4\rangle), \\ |\tilde{\psi}_{\overline{111}}^{(\prime)}\rangle &= \frac{1}{2}(|\phi_1\rangle \pm |\phi_2\rangle \mp |\phi_3\rangle \mp |\phi_4\rangle), \\ |\tilde{\psi}_{1\overline{11}}^{(\prime)}\rangle &= \frac{1}{2}(|\phi_1\rangle \mp |\phi_2\rangle \pm |\phi_3\rangle \mp |\phi_4\rangle), \\ |\tilde{\psi}_{11\overline{1}}^{(\prime)}\rangle &= \frac{1}{2}(|\phi_1\rangle \mp |\phi_2\rangle \mp |\phi_3\rangle \pm |\phi_4\rangle),\end{aligned} \tag{A7}$$

where $i=1,\ldots,4=(111),\ldots,(\overline{111})$. Using the $\tilde{O}$ transformation and Eq. (A2), we get for the $\langle \tilde{\psi}_i | \mathbf{r} | \tilde{\psi}_j \rangle$ matrix elements

$$\frac{1}{2}\begin{pmatrix} (\lambda+\delta)(\mathbf{i}+\mathbf{j}+\mathbf{k}) & (\lambda-\delta)\mathbf{i} & (\lambda-\delta)\mathbf{j} & (\lambda-\delta)\mathbf{k} \\ (\lambda-\delta)\mathbf{i} & (\lambda+\delta)(\mathbf{i}-\mathbf{j}-\mathbf{k}) & -(\lambda-\delta)\mathbf{k} & -(\lambda-\delta)\mathbf{j} \\ (\lambda-\delta)\mathbf{j} & -(\lambda-\delta)\mathbf{k} & (\lambda+\delta)(-\mathbf{i}+\mathbf{j}-\mathbf{k}) & -(\lambda-\delta)\mathbf{i} \\ (\lambda-\delta)\mathbf{k} & -(\lambda-\delta)\mathbf{j} & -(\lambda-\delta)\mathbf{i} & (\lambda+\delta)(-\mathbf{i}-\mathbf{j}+\mathbf{k}) \end{pmatrix}. \tag{A8}$$

We note that taking the $\widetilde{O'}$ transformation corresponds to changing λ into $-\lambda$ in Eq. (A8) for the $\langle \tilde{\psi}'_i | \mathbf{r} | \tilde{\psi}'_j \rangle$ matrix elements. Using this latter equation, together with Eq. (A6), we obtain the total spreads of the $|\tilde{\psi}_i\rangle$ and $|\tilde{\psi}'_i\rangle$ WF's,

$$\begin{aligned}\Omega_{\tilde{\psi}} &= \sum_i \left[\langle \tilde{\psi}_i | r^2 | \tilde{\psi}_i \rangle - |\langle \tilde{\psi}_i | \mathbf{r} | \tilde{\psi}_i \rangle|^2\right] \\ &= \Omega_s + 3\Omega_p - 3(\delta+\lambda)^2 = \Omega_\phi - 3(\delta+\lambda)^2 \leqslant \Omega_\phi\end{aligned} \tag{A9}$$

and

$$\Omega_{\tilde{\psi}'} = \Omega_\phi - 3(\delta-\lambda)^2 \leqslant \Omega_\phi . \tag{A10}$$

Two cases have to be considered according as δ is zero (point groups T_h, O, O_h) or not (point groups T and T_d).

If $\delta=0$, the two spreads $\Omega_{\tilde{\psi}}$ and $\Omega_{\tilde{\psi}'}$ are both equal to $\Omega_\phi - 3\lambda^2$. We demonstrate first that this latter value is the minimum of the spread, Eq. (A6). To this end, using Eqs. (A2) and (A4), and the orthonormality conditions $\Sigma_j O_{ij}^2 = 1$ and $\Sigma_i O_{i1}^2 = 1$, we are led to minimizing

$$\begin{aligned}\Omega_\psi &= \Omega_\phi - 4\lambda^2 \sum_i O_{i1}^2 (O_{i2}^2 + O_{i3}^2 + O_{i4}^2) \\ &= \Omega_\phi - 4\lambda^2 + 4\lambda^2 \sum_i O_{i1}^4 ,\end{aligned} \tag{A11}$$

with the constraint

$$C=\sum_i O_{i1}^2-1=0. \tag{A12}$$

The conditions for an extremum of Ω_ψ, introducing the Lagrangian multiplier Λ are

$$\frac{\partial\Omega_\psi}{\partial O_{i1}}+\Lambda\frac{\partial C}{\partial O_{i1}}=16\lambda^2O_{i1}^3+2\Lambda O_{i1}=0, \tag{A13}$$

from which we get

$$O_{11}^2=O_{21}^2=O_{31}^2=O_{41}^2=\frac{1}{4}, \tag{A14}$$

and the result

$$\min\Omega_\psi=\Omega_\phi-3\lambda^2=\Omega_{\tilde\psi}\equiv\Omega_{\tilde\psi'}\leqslant\Omega_\phi. \tag{A15}$$

We demonstrate next that in addition to $\tilde O$ and $\widetilde{O'}$, there is in fact an *infinity* of orthogonal transformations producing $|\psi_i\rangle$ orbitals with this same minimum spread value. For this purpose, we introduce the operator $R(\alpha,\beta,\gamma)$ corresponding to a geometrical rotation specified by its Euler angles, and its three-dimensional unitary representation $D^{(1)}(\alpha,\beta,\gamma)_{mm'}$, whose basis functions are the spherical harmonics Y_{1m}, with $m=1,0,-1$. Consistently with our choice of the basis functions $|\phi_2\rangle$, $|\phi_3\rangle$, and $|\phi_4\rangle$, we consider instead the equivalent, real orthogonal representation $D^{(1)}(\alpha,\beta,\gamma)_{\xi\xi'}$ with $\xi,\xi'=x,y,z$, which is the usual transformation of the Cartesian coordinates of a vector. We then build from this matrix the following orthogonal transformation acting in the four-dimensional Hilbert space $\mathcal{H}_4$,

$$\mathcal{D}(\alpha,\beta,\gamma)=\begin{pmatrix}1 & 0 & 0 & 0\\ 0 & & & \\ 0 & & D^{(1)}(\alpha,\beta,\gamma)_{\xi\xi'} & \\ 0 & & & \end{pmatrix}. \tag{A16}$$

We write $|\hat\psi_i\rangle=\Sigma_k\tilde O_{ik}\Sigma_j\mathcal{D}(\alpha,\beta,\gamma)_{kj}|\phi_j\rangle$, and get after some algebra, using Eqs. (A2) and (A4),

$$\Omega_{\hat\psi}\equiv\Omega_{\tilde\psi}=\Omega_\phi-3\lambda^2\quad\forall\alpha,\beta,\gamma. \tag{A17}$$

It is important to remember that the $|\phi_i\rangle$ are basis functions of irreducible representations of a cubic group, and *not* of the full rotation group. Therefore, applying the transformation (A16) on the original basis functions $|\phi_i\rangle$ does not result in rotated $\phi_i(\mathbf{r})$ functions, i.e., $\phi_i(R^{-1}(\alpha,\beta,\gamma)\mathbf{r})$, but in linear combinations of the original basis functions, defining the same Hilbert space $\mathcal{H}_4$, and carrying the same chemical information as the original functions.

When $\delta\neq0$ (case of T and T_d), the two transformations $\tilde O$ and $\tilde O'$ produce $|\tilde\psi_i\rangle$ and $|\tilde\psi_i'\rangle$ orbitals with different total spreads

$$\begin{aligned}&\Omega_{\tilde\psi}<\Omega_{\tilde\psi'}\quad\text{if}\quad\delta>0\quad(\lambda\delta\geqslant0)\\ &\Omega_{\tilde\psi}>\Omega_{\tilde\psi'}\quad\text{if}\quad\delta<0\quad(\lambda\delta\leqslant0).\end{aligned} \tag{A18}$$

We prove finally that $\Omega_{\tilde\psi}$ for $\delta>0$ (or $\Omega_{\tilde\psi'}$ for $\delta<0$) is a local minimum of the total spread. To this end, we consider an infinitesimal orthogonal transformation of the $|\tilde\psi_i\rangle$ (or $|\tilde\psi_i'\rangle$)

$$O(\epsilon)=I+\epsilon A+\frac{1}{2}\epsilon^2A^2+O(\epsilon^3), \tag{A19}$$

where A is an antisymmetrical operator defined by 6 real parameters. Using Eq. (A8) and applying Eq. (A19) to the sets of sp^3 hybrid orbitals $|\tilde\psi_i\rangle$ and $|\tilde\psi_i'\rangle$, we obtain for the infinitesimal variations of the spreads, up to second-order terms in ϵ, positive semi-definite quadratic forms in the parameters of the A operator. Hence the correction to $\Omega_{\tilde\psi}$ ($\Omega_{\tilde\psi'}$) induced by the infinitesimal transformation, are non-negative. The spread $\Omega_{\tilde\psi}$ ($\Omega_{\tilde\psi'}$) therefore corresponds for $\delta>0$ ($\delta<0$) to a local minimum of the localization functional.

*Electronic address: postma@dpmail.epfl.ch

[1] G. H. Wannier, Phys. Rev. **52**, 191 (1937).
[2] S. F. Boys, in *Quantum Theory of Atoms, Molecules, and the Solid State*, edited by P. O. Löwdin (Academic Press, New York, 1966), p. 253.
[3] N. Marzari and D. Vanderbilt, Phys. Rev. B **56**, 12 847 (1997).
[4] K. Terakura, T. Oguchi, A. R. Williams, and J. Kübler, Phys. Rev. B **30**, 4734 (1984).
[5] W. L. Roth, Phys. Rev. **110**, 1333 (1958).
[6] S. Massidda, M. Posternak, A. Baldereschi, and R. Resta, Phys. Rev. Lett. **82**, 430 (1999).
[7] A. Svane and O. Gunnarsson, Phys. Rev. Lett. **65**, 1148 (1990); Z. Szotek, W. M. Temmerman, and H. Winter, Phys. Rev. B **47**, 4029 (1993).
[8] V. I. Anisimov, J. Zaanen, and O. K. Andersen, Phys. Rev. B **44**, 943 (1991).
[9] S. Massidda, A. Continenza, M. Posternak, and A. Baldereschi, Phys. Rev. Lett. **74**, 2323 (1995).
[10] S. Massidda, A. Continenza, M. Posternak, and A. Baldereschi, Phys. Rev. B **55**, 13 494 (1997).
[11] N. Marzari and D. Vanderbilt, in *First-Principles Calculations for Ferroelectrics: Fifth Williamsburg Workshop*, edited by R.E. Cohen (AIP, Woodbury, NY, 1998), p. 146.
[12] I. Souza, R. M. Martin, N. Marzari, X. Zhao, and D. Vanderbilt, Phys. Rev. B **62**, 15 505 (2000).
[13] H.J.F. Jansen and A.J. Freeman, Phys. Rev. B **30**, 561 (1984).
[14] S. Massidda, M. Posternak, and A. Baldereschi, Phys. Rev. B **48**, 5058 (1993).
[15] A. B. Shick, A. I. Liechtenstein, and W. E. Pickett, Phys. Rev. B **60**, 10 763 (1999).
[16] D. Singh, Phys. Rev. B **43**, 6388 (1991).
[17] J. B. Goodenough and A. Hamnett, in *Zahlenwerte und Funktionen aus Naturwissenschaften und Technik*, edited by O. Madelung, Landolt-Börnstein, New Series, Group III, Vol. 17g (Springer, New York, 1984), p. 201.
[18] H. J. Monkhorst and J. D. Pack, Phys. Rev. B **13**, 5188 (1976).

[19] E. Krüger, Phys. Status Solidi B **52**, 215 (1972); **52**, 519 (1972).
[20] G. F. Koster, J. O. Dimmock, R. G. Wheeler, and H. Statz, *Properties of the Thirty-two Point Groups* (MIT Press, Cambridge, 1963).
[21] R. D. King–Smith and D. Vanderbilt, Phys. Rev. B **47**, 1651 (1993).
[22] M. Posternak, A. Baldereschi, H. Krakauer, and R. Resta, Phys. Rev. B **55**, R15 983 (1997).